Chapter 4

Synaptogenic control of the shape of dendritic filopodia

4.1 Abstract

Filopodia are thin and long protrusions that predominantly occur on developing neurons in the CNS. Axonal filopodia are shown to mediate diverse processes such as detedting surface molecules and sensing chemical gradients. In contrast, the role of dendritic filopodia is poorly understood. We used high resolution confocal microscopy and precise 3-dimensional reconstruction of dendritic filopodia to investigate the function of dendritic filopodia during postembryonic remodelling of the Motorneuron 5 in *Manduca sexta*. We show that, upon emergence at the onset of dendritic growth, filopodia undergo a morphogenic reduction in length and branching complexity during ongoing postembryonic development. Length, branching complexity and structural variability of filopodia at dendritic tips however are greater than at dendritic shaft regions. Tip filopodia are constant in density, whereas shaft filopodia density is developmentally reduced. We further analyzed the localized relation of immuno-labeled presynaptic profiles to dendritic filopodia and demonstrate a developmental translocation of putative presynaptic profiles along dendritic shaft filopodia towards the postsynaptic dendrite. We discuss these results and can show that at least two functionally distinct types of filopodia exist within the same dendritic tree: tip filopodia might primarily be involved in the process of steering dendritic growth, whereas shaft filopodia might serve as guiding structures that direct the growth of presynaptic axons towards postsynaptic dendrites.

4.2 Introduction

One of the fascinating and still unresolved questions in developmental neuroscience is how neurons in the central nervous system find their correct partners among the myriad of neurons, wire together and build functional neuronal circuits. Filopodia, thin and highly motile actin-rich cell surface protrusions found in a rich variety of organisms are thought to be one of the essential structures that mediate (i) steering of axonal and dendritic growth cones and (ii) initial probing with other neurons. To date neuronal filopodia have primarily been studied with respect to axonal pathfinding (Gomez et al., 2001; Kater and Shibata, 1994; Portera-Cailliau et al., 2003; Rehder and Kater, 1992, 1996; Robles et al., 1999) and synaptogenesis (Fiala et al., 1998; Konur and Yuste, 2004; Lohmann et al., 2005; Niell et al., 2004; Portera-Cailliau et al., 2003; Vaughn, 1989; Yuste and Bonhoeffer, 2004; Ziv and Smith, 1996). The nearly ubiquitous appearance of filopodia on migrating cells suggests an evolutionary ancient origin. However, the mechanisms that regulate filopodial movement and appearance may have diverged during evolution. For example, presynaptic activity has been demonstrated to regulate dendritic filopodia during early embryogenesis (Lohmann et al., 2005), however filopodial shape of axonal growth cone filopodia can be controlled by contact with cell surface molecules (Gomez et al., 2001).
Tremendous technical advances in live imaging of growing neurons have provided some understanding about the regulation of filopodial appearance. Neuronal activity affects filopodial shape and motility at axonal growth cones (Gomez et al., 1999, 2001; Gomez and Spitzer, 2000) and dendrites (Lohmann et al., 2005; Portera-Cailliau et al., 2003), and synaptic contacts have been shown to stabilize dendritic filopodia (Konur and Yuste, 2004; Lohmann et al., 2005; Niell et al., 2004). However, such morphological changes have been followed only for short periods during development. Filopodial morphogenesis over longer periods of development has thus far only been investigated in pyramidal cells of rat visual cortex (Portera-Cailliau et al., 2003). These studies demonstrated morphologically distinct types of filopodia at dendritic tip and shaft regions, which respond differentially to induced neuronal activity. To date we understand relatively little of how different dendritic filopodial types participate in steering of neuritic growth, sampling of axons and synaptogenesis in central nervous system during development.
Insect metamorphosis provides a compelling example of dendritic and synaptic remodelling since larval and adult behaviors place different demands on the CNS (Consoulas et al., 2000; Tissot and Stocker, 2000). This study is the first to investigate the role of filopodia in postembryonic remodelling of neuronal architecture in the intact central nervous system. As model we use the morphogenesis of the identified Motorneuron 5 of

the hawkmoth *Mandua sexta*. At the end of larval life, synapses of the larval circuitry are dismantled as the neuron retracts its dendrites (Duch and Levine, 2000; Duch and Mentel, 2004). Subsequently, during (and limited to) the initial phase of rapid dendritic outgrowth and synaptogenesis, filopodia densely decorate the neuron's dendritic surface. During the second growth phase in the ensuing 2 weeks of development, dendritic growth is restricted to higher order branches (Libersat and Duch, 2002). Metamorphosis is controlled by ecdysteroids, and the ecdysteroid 20-hydroxyecdysone (20HE) has been demonstrated to influence dendritic shape (Levine et al., 1995; Levine and Weeks, 1996; Truman, 1990; Weeks and Truman, 1986) and promote filopodia elongation and branching (Matheson and Levine, 1999). Factors that induce shortening of dendritic filopodia in insects have not been identified. In vertebrates, filopodial shape has been suggested to be under the control of synaptogenesis (Lohmann et al., 2005). In this study, we address two questions: First, how does filopodial shape change during insect metamorphosis? Secondly, how does this process relate to or co-operate with synaptogenesis?

In the first instance, we analyze the morphogenic fate of filopodia during postembryonic development using novel accurate 3-dimensional reconstruction methods (Evers et al., 2005) in conjunction with quantitative metric analyses. In the second part, we investigate the interplay of postsynaptic filopodia with putative presynaptic sites. To achieve this, we employ novel quantification strategies of 3-dimensional co-localization analysis for immuno-cytochemically labeled presynaptic specializations along postsynaptic filopodial projections.

We demonstrate that filopodial length and branching complexity is gradually reduced during the initial phase of massive dendritic outgrowth. Dendritic shaft filopodia are significantly shorter than tip filopodia and their morphology is under tighter regulation than that of tip filopodia. At the beginning of the second dendritic growth phase, the core architecture of the dendritic field is laid out and dendritic branching is restricted to the perimeter (Libersat and Duch, 2002). Concomitantly, filopodia disappear with only few remaining that are sparsely distributed over the dendritic field. We further demonstrate a developmental translocation of immuno-cytochemically visualized synaptotagmin profiles along filopodia towards the purely postsynaptic dendrite, and that this process takes place along filopodia at stable dendritic shafts. We discuss these results and can show, that tip filopodia might primarily be involved in the process of steering dendritic growth, whereas shaft filopodia might serve as guiding structures that direct the growth of presynaptic axons towards postsynaptic dendrites.

4.3 Materials and Methods

4.3.1 Animals rearing and staging

Manduca sexta (L) obtained from a laboratory culture were reared on artificial diet (Bell and Joachim, 1976) under a long-day photoperiod regime (17/7 hr light/dark cycle) at 26°C. Both chronological and morphological criteria were used for staging of animals (Bell and Joachim, 1976; Reinecke et al., 1980; Tolbert et al., 1983). Dissection and intracellular recording were performed as described in Duch and Levine (2000).

4.3.2 Intracellular labelling, Immuno-Cytochemistry and sample preparation

A glass microelectrode (20-25 MOhm) was filled with 7 % Neurobiotin in 2 M potassium acetate to fill the Motorneuron 5 of *Manduca sexta* intracellularly by injection of 3nA depolarizing current for 45 minutes. The ganglia were fixed with 4% Paraformaldehyde at 7°C for 2 hours, rinsed for 1h in phosphate buffer (PBS), dehydrated in an ascending ethanol series (50, 70 90, 100%, 15 minutes each) and subjected to lipid extraction in series of 1:1 Ethanol/Methylsalicylate, 100% Methylsalicylate, and 1:1 Methylsalicylate/xylol for 10 minutes each to increase antibody permeability and reduce background staining. Subsequently, these steps were executed in reverse order. After rehydration in a descending ethanol series the ganglia were bathed in 0.5% TritonX PBS for 2 hours. For immuno-labeling, ganglia were pre-incubated in 10% normal goat serum 0.5% TritonX PBS for 1 hour, incubated in primary antibody (Rabbit anti-synaptotagmin) for 2 days, and washed in PBS for 1 hour. The synaptotagmin antibody was a gift from Dr. L. P. Tolbert (ARL Division of Neurobiology, University of Arizona,Tucson, AZ). It had been raised against the unique N terminus of *Manduca sexta* synaptotagmin and has been shown to specifically detect *Manduca* synaptotagmin (Dubuque et al., 2001).
Neurobiotin was visualized using Cy3-steptavidin (Jackson Immunochemicals Inc.; 1:750 in 0.05% TritonX PBS), co-applied with Cy5-coupled Mouse anti-Rabbit (Jackson Immunochemicals Inc.) secondary antibody (1:200). After wash in PBS for 1 hour, the preparation was dehydrated, cleared and mounted in 100% Methylsalicylate. Acquisition of confocal image stacks was done immediately.

4.3.3 Image acquisition

We used a Leica (Bensheim,Germany) TCS SP2 laser scanning microscope to acquire image stacks of double labeled preparations. All images were obtained with Leica HCX PL APO CS 40X oil immersion objective (numerical aperture, 1.25) in simultaneous acquisition mode, i.e. the emitted fluorescence light of synchronously excited fluorophores was divided by an acoustic-optical beam splitter to be detected by separate photomultipliers. Thus, no image misalignment occurred due to error in scan mirror positioning. To correct for chromatic aberration, a neuron was filled with biotin and double labeled with Cy3- and Cy5-coupled streptavidin (Jackson ImmunoResearch). An image stack was obtained as described above. The misalignment between both structures was measured and applied onto later acquired image stacks of equally treated specimens (Wouterlood et al., 1998).

4.3.4 Image analysis and statistical evaluation

Confocal image stacks were further processed with Amira-3.1.1 software (TGS). For 3-dimensional reconstruction of dendritic segments and filopodia, self-developed software was used, delivering precise quantification of midline and diameter as well as a triangulated surface definition fully exploiting optical resolution (Evers et al., 2005; Schmitt et al., 2004). For quantification of the distribution of immuno-labeled profiles along filopodia, the generated surface description was used to calculate the staining density within 300nm from each surface element, a triangle. The position of the triangle was determined perpendicular to the midline of the corresponding reconstructed segment. For details, see Evers et al. (2005). Snapshots of scenes rendered in Amira-3.1.1 are arranged into figures with Adobe Illustrator and Photoshop CS (Adobe Systems Incorporated).
For statistical analyses, morphological parameters were imported into R (R Development Core Team, 2004) from ASCII-tables generated in Amira. Filopodia length metrics are statistically tested with pairwise Wilcoxon rank sum test. Student's t-Test was used for pairwise comparison of mean filopodia density between dendritic shaft and tip regions at specific stages.

4.4 Results

4.4.1 Metamorphic reorganisation of Motorneuron 5 dendritic tree

During postembryonic development, the MN5 grows in two different modes of branch formation: following the regression of the larval tree in late larval life until pupal stage 2, the neuron shows an initial phase of massive dendritic outgrowth during pupal stage 3 (Fig. 4.1*A*), 4 (Fig. 4.1*B*) and 5 (Fig. 4.1*C*), in a way that all major adult dendrites are already laid out during the first three days of dendritic growth. During the subsequent 2 weeks of pupal development, addition of new branches is restricted to high order branches at the dendritic perimeter (Libersat and Duch, 2002).
During the first phase of rapid dendritic outgrowth, filopodia (Fig. 4.1*D-I*, exemplarily marked with arrows) are found distributed all over the dendritic tree at tip (*D-F*) and shaft (*G-I*) regions. Filopodia are recognized by their low staining intensity and their exceptional small radius compared to dendrites (Yuste and Bonhoeffer, 2004). They are formed within a few hours during the transition from pupal stage 2 to 3 and span a volume which roughly covers the dimensions of the dendritic field at pupal stage 5 (data not shown). During ongoing filopodia dependent dendrite formation the overall filopodium density seems to be reduced.
During pupal stages 3 to 5, not a single dendritic tip can be found without filopodia, clearly showing filopodia dependent dendritic growth. Entering pupal stage 6, the dendritic field is laid out and the frequency of filopodia-like protrusions is drastically reduced, so that filopodia occur only sporadically at dendritic tips as well as dendritic shafts and hence elude statistic analysis. Filopodia can not be found at the somatic region or the primary link segment outside the neuropil area at any point of time during postembryonic development.

4.4.2 Morphology of filopodia

Dendritic filopodia have a very small radius (mean 0.20μm, sd 0.05μm), however they show a great variability in their branch structure. Straight filopodia with lengths ranging from 1 to more than 10 μm are intermingled with complex branching filopodia with more than 5 branchpoints and maximum path length longer than 20μm. However, already by visual inspection filopodia at dendritic shafts seem to be less variable in shape and projection length. To explore this quantitatively, precise 3-dimensional reconstruction (Evers et al., 2005) of filopodia at dendritic tips as well as dendritic shafts are conducted

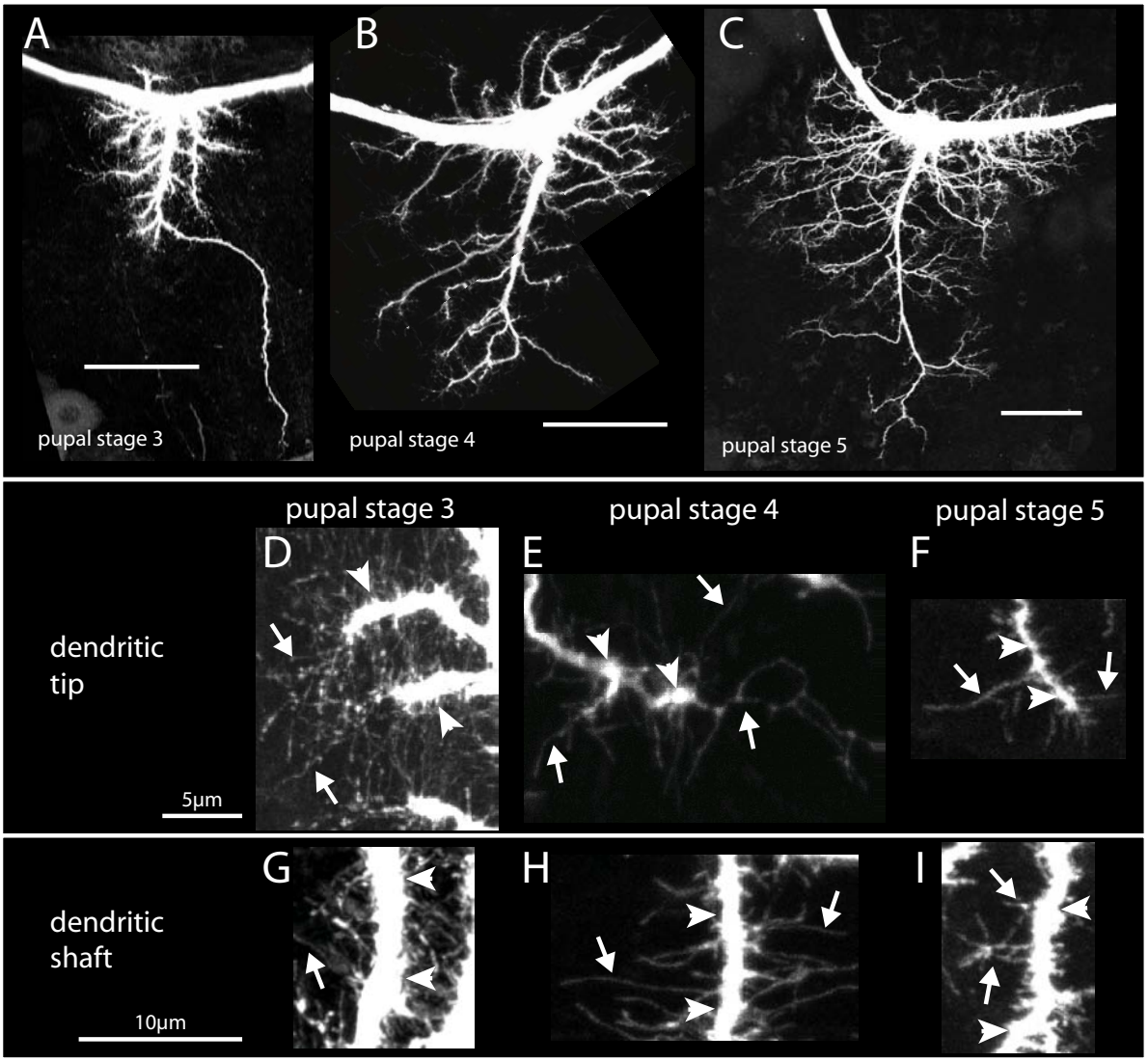

Figure 4.1: The first phase of massive dendritic outgrowth is filopodia dependent in the Motorneuron 5 (MN5) of *Manduca sexta*. *A* At pupal stage 3, following the maximum dendrite retraction after pupation, the MN5 starts outgrowth, concomitant with filopodia (arrows) protruding densely packed from the neuron's surface at tip (*D*) and shaft (*G*) dendrites (arrow heads). *B* MN5 at pupal stage 4. During fast dendritic outgrowth, filopodia are found at all dendritic tips (*E*) and shaft regions (*H*). Filopodia at dendritic tips (*E*) appear more branched and more variable in length than at shaft regions (*H*). *C* At pupal stage 5, all major central dendrites found later in the adult animal are laid out. This stage is the last during development at which filopodia can be found regularly distributed over the dendritic tree at tip (*F*) and shaft (*I*) regions. However, filopodia appear to be shorter and less branched compared to previous developmental stages. *A*-*C* scalebars = 50 μm.

at pupal stages 3, 4 and 5. Filopodia originating within the last 5μm of a dendrite are classified as tip filopodia. Shaft filopodia are taken from straight, non-branched and at least 10μm long segments between dendrite branchpoints to confine the analyses to a most possible uniform type, and to exclude filopodia involved in the formation of interstitial branching.

Fig. 4.2 shows representative examples of reconstructions of filopodia (*yellow*) at tip (*A*-*C*) and shaft (*D*-*F*) locations of dendritic segments (*red*, scale bar is 10μm). The corresponding dendrograms are depicted in Fig. 4.2*G* (tip filopodia) and 4.2*H* (shaft filopodia; scale bar is 20μm) for each stage. Their spatial appearance in 3 dimensions is illustrated by depicting the same reconstruction in three different views: top-view (*left*), along the dendritic axis (*right top*), and side-view (*right bottom*). A dendritic tip from a pupal stage 3 preparation (Fig. 4.2*A*) bears the farthest reaching filopodia with the most complex branching structure, which can be judged best from the dendrogram (Fig. 4.2*F left*). One day later in development, at pupal stage 4, the representative dentritic tip (Fig. 4.2*B*) shows filopodia which are shorter and less branched than in pupal stage 3 (Fig. 4.2*A*). However, some individual filopodia with complex branching pattern and high length still occur. A dendritic tip reconstruction at pupal stage 5 shows the shortest filopodia few of which are branched (Fig. 4.2*C*). In summary, dendritic tip filopodia length and branching complexity decreases during ongoing rapid dendritic growth between pupal stages 3 and 5. The same is the case for dendritic shaft filopodia. However, in comparison to tip filopodia the developmental decrease of length and branch number of shaft filopodia is less severe (pupal stage 3, Fig. 4.2*D*; pupal stage 4, Fig. 4.2*E*; pupal stage 5, Fig. 4.2*F*). Another difference between tip and shaft filopodia is that at dendritic shafts length and number of branches per filopodium are smaller than at dendritic tips from the same neuron (compare Fig. 4.2*G* and *H*). Beginning with pupal stage 6 filopodia are sparsely distributed over the dendritic arbor so that single filopodia can only be found sporadically within 10μm dendritic length and therefore are not further analyzed in this work.

Taken together, dendritic filopodia undergo a developmental morphogenesis and the different morphometric attributes within given stages suggest the existence of qualitatively different types of filopodia at dendritic tips and at dendritic shafts of the same neuronal tree. For statistical analysis of these phenomena, the following three parameters describing filopodia shape are selected: (i) total path length (TPL, i.e. summed length of all filopodia branches arising from the same first order segment originating at dendritic shaft or tip), maximum path length (MPL, i.e. the path from the root of the filopodium to the furthermost tip along the segments midline) and segment length (SL, length of indi-

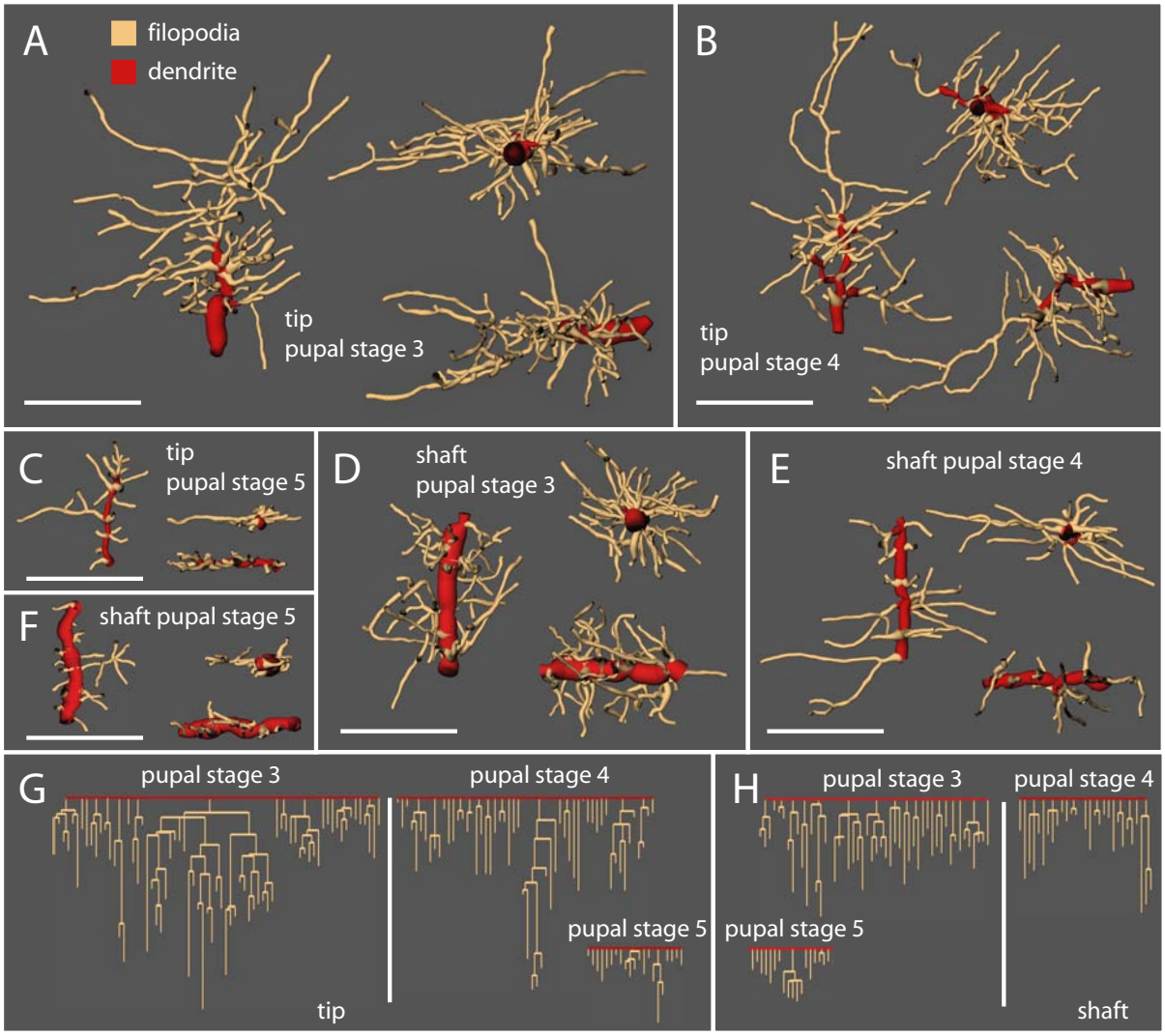

Figure 4.2: Quantification of filopodia morphology by precise 3-dimensional reconstructions. Representative reconstructions of dendritic tip (*A*-*C*) and shaft (*D*-*F*) regions are exemplarily shown in 3 different perspectives in each panel (*left*: top view; *right top*: axial view; *right bottom*: side view), illustrating the spatial stretch out of filopodia (*yellow*) originating at dendritic segments (*red*). Dendrograms of the reconstructions are shown in *G* (dendritic tips) and *H* (dendritic shafts). The farthest reaching filopodia with highest branching complexity originate at the dendritic tip at pupal stage 3 (*A*, *G*). During the subsequent 2 developmental stages, tip filopodia length and branching complexity is reduced (*B*, pupal stage 4; *C*, pupal stage 5) (see dendrograms in *G*). The same is true for shaft filopodia: length and branching complexity of filopodia is reduced during pupal stages 3 (*D*), 4 (*E*) and 5 (*F*). Comparing the dendrograms of tip (*G*) and shaft (*H*) regions, shaft filopodia seem to be shorter and less branched than their counterparts at tip regions at the respective developmental age. *A*-*F*: scalebar is 10 μm. *G*, *H*: scalebar is 20 μm.

vidual segments between branchpoints/endpoints). TPL accounts for the sensing length of a filopodium to sample the surrounding neuropil, MPL however indicates the distance a filopodium reaches from the dendrite into the neuropil, and SL helps to analyze the preferred growth length before a filopodium branches.
These parameters are shown as box and whisker plots in Fig. 4.3. The left edge of the rectangle is at the 1^{st} quartile, the right edge at the 3^{rd} quartile. The median is plotted as vertical line within the box. The whiskers extend up to the 1.5× range between median and 1^{st} quartile, and the 3^{rd} quartile respectively, if data is within this range. Extreme values outside this interval are plotted as circles. The x-axis is scaled logarithmically.

4.4.3 Filopodia total path length is significantly reduced during development

In Fig. 4.3*A* the total path length (TPL) of filopodia is analyzed separately for each developmental stage and localization (tip versus shaft) within the dendritic tree. Pupal stage 3 tip filopodia exhibit the biggest span of TPL (n=304 filopodia, N=16 dendritic segments), ranging from minimum (min) 0.47μm to maximum (max) 146.5μm with the median at 6.0μm (mean 12.5μm, sd 17.4μm). One day later in development (pupal stage 4), TPL of tip filopodia is significantly reduced (n= 383, N=20; min 0.4 μm; max 78.1μm; median 4.13; mean 7.6μm; sd 9.5μm; $p < 0.05$). This decrease of tip filopodia TPL continues to pupal stage 5 (n= 392; N=36; min 0.3μm; max 40.4μm; median 2.5μm; mean 4.3μm; sd 4.9μm), which differs highly significantly from TPL in pupal stages 3 and 4 ($p < 0.0001$).
Shaft filopodia also show a statistically significant ($p < 0.001$) developmental decrease in TPL from pupal stages 3 (n= 281; N=15; min 0.3μm; max 30.9μm; median 4.5μm; mean 5.9μm; sd 5.0μm) through stage 4 (n= 276; N=23; min 0.3μm; max 24.6μm;median 3.4μm;mean 4.5μm;sd 3.8μm) until pupal stage 5 (n= 215; N=11; min 0.6μm; max 19.3μm; median 2.3μm; mean 3.2μm; sd 2.7μm). Therefore, both tip and shaft filopodia undergo significant shortening during dendritic field development. However, comparing TPL of shaft and tip filopodia, shaft filopodia are significantly ($p < 0.001$) shorter than their corresponding counterpart at dendritic tips at pupal stages 3 and 4.

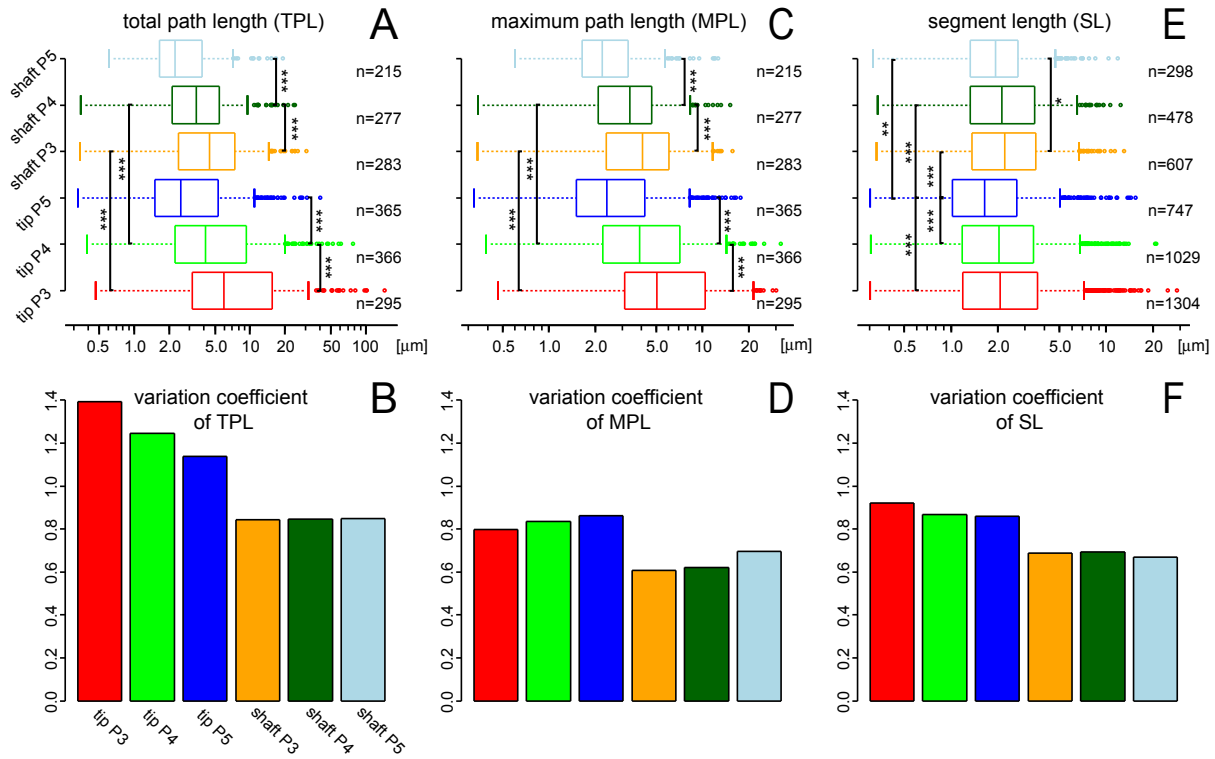

Figure 4.3: Developmental change of filopodia shape: evidence for distinct filopodia at dendritic tip and shaft regions. Continued on next page.

4.4.4 Regulation tightness of filopodia total path length increases during development

In pyramidal neurons from acute slices of mouse neocortex, live cell multi-photon imaging has recently demonstrated that the motility and length of filopodia are greater in dendritic tips than in dendritic shafts, and that both types of filopodia are regulated by different mechanisms (Portera-Cailliau et al., 2003). One hint for different regulatory mechanisms for tip and shaft filopodia also in insect neurons would be a different regulation tightness. We use the variation coefficient (VC, standard deviation / mean) as a measure for the tightness of filopodia shape regulation. It gives the relative broadness of a distribution and therefore reflects the degree of regulation, so that smaller VC indicates tighter regulation of the parameter under investigation. The VC of TPL is calculated at pupal stages 3, 4 and 5 for shaft as well as tip filopodia and plotted in Fig. 4.3*B*. The VC of tip filopodia is reduced with ongoing development, indicating that the regulation of TPL of tip filopodia shape gets tighter with maturation of these structures. Shaft filopodia, however, have a noticeable smaller VC compared to tip filopodia, reflecting an overall narrower growth regulation. They furthermore do not exhibit a change of VC during

Figure 4.3: continued

A Total path length (TPL), i.e. length of all branches of individual filopodia, is significantly reduced during developmental morphogenesis of filopodia at dendritic tips and shaft. Shaft filopodia have significantly shorter TPL than tip filopodia at pupal stages 3 and 4. The variability of TPL, i.e. regulation strength, is assessed by the variation coefficient (VC; standard deviation form mean/mean), plotted in *B*. VC of TPL gets smaller during development at tip regions, indicating increasing regulation strength. Regulation strength of shaft filopodia TPL, however stays constant. *C* To separate two distinct phenomena, filopodia branching width and projection reach, the maximum path length (MPL), i.e. the path length from the dendritic origin to the farthest reaching tip of individual filopodia, is evaluated. MPL is significantly different between tip and shaft filopodia at pupal stages 3 and 4 and is down-regulated during development at tip and shaft regions. VC of MPL (*D*) varies only in small ranges at tip and shaft regions and is smaller at shaft filopodia compared to tip filopodia. *E* Segment length (SL), i.e. the path between branch/endpoints of filopodia. SL does not differ between tip and shaft filopodia, except for tip filopodia at pupal stage 5 which is significantly shorter compared to all other stages and locations.. At shaft filopodia, SL is not reduced between subsequent developmental stages, but is significantly shortened between pupal stage 3 and 5. *F* variation coefficient of SL. The variability of SL at shaft filopodia is smaller than of tip filopodia. To conclude, shaft and tip filopodia significantly differ and undergo morphogenesis, but shaft filopodia underlie a stronger regulation. Box and whisker plots in *A,C* and *E*: the rectangle's left edge indicates 1^{st} quartile, right edge the 3^{rd} quartile; median is at the vertical line within the box. Whiskers extend to data points within 1.5× the range between median and 1^{st} quartile, and 3^{rd} quartile respectively. Circles = extreme values. The x-axis is scaled logarithmically. *p<0.05; **p<0.01; ***p<0.001.

development, indicating a different regulation of shape of filopodia at different locations within the dendritic tree.

4.4.5 Filopodia maximum path length is significantly reduced during development

As demonstrated by representative examples of shaft and tip filopodia for each developmental stage (Fig. 4.2), not only filopodia length, but also filopodia branching complexity is decreased during ongoing dendritic growth. The quantification of TPL (Fig. 4.3*A*) accounts for both, length and branching complexity, which in fact might be regulated by different mechanisms. To look at length only we also quantified the maximum path length (MPL) of tip and shaft filopodia for each stage, i.e. from the foot to the furthermost filopodium tip (Fig. 4.3*C*). MPL shows the same developmental reduction as TPL (Fig. 4.3*A*) at tip and shaft locations, but it spans a smaller range. MPL of pupal stage 3 tip filopodia is longest (n=304; N=16; min 0.5μm; max 30.2μm; median 5.1μm; mean

7.2μm; sd 5.8μm), decreases to pupal stage 4 (n=383; N=20; min 0.4μm; max 32.5μm; median 3.9μm; mean 5.3μm; sd 4.5μm) and is shortest at pupal stage 5 (n=392; N=36; min 0.3μm; max 17.7μm; median 2.4μm; mean 3.5μm; sd 3.0μm).
MPL of shaft filopodia is significantly shorter ($p<0.001$) than of tip filopodia at pupal stages 3 and 4, but is also significantly ($p<0.001$) down regulated during development from pupal stage 3 (n=281; N=15; min 0.3μm; max 15.7μm; median 4.1μm; mean 4.6μm; sd 2.8μm) through pupal stage 4 (n=276; N=23; min 0.3μm; max 15.1μm; median 3.4μm; mean 3.7μm; sd 2.3μm) until pupal stage 5 (n=215; N=11; min 0.6μm; max 12.7μm; median 2.2μm; mean 2.9μm; sd 2.0μm).
Calculating the VC of the distribution of MPL reveals no obvious change of regulation tightness during development neither of tip nor of shaft filopodia (Fig. 4.3D), in contrast to TPL of tip filopodia, which undergoes a developmental tightening. However shaft filopodia exhibit a smaller VC than tip filopodia. This once more underlines a stronger regulation of shaft filopodia than tip filopodia shape. Comparing VC of TPL and MPL shows a tighter regulation of the maximum projection length of filopodia than of their branch behavior.

4.4.6 Collective collapse of only tip filopodia at pupal stage 5

As MPL is reduced less than TPL, the developmental decrease in filopodia TPL goes along with a reduction in filopodia branching. To test whether this is accompanied by degenerative events like collective filopodia regression or collapse, the segment length (SL, length of all individual segments between branchpoints/endpoints) of tip and shaft filopodia is quantified for each developmental stage (Fig. 4.3E). The data show that filopodial SL is not shortened at shaft regions between subsequent developmental stages, irrespective of significant reductions in TPL and MPL through the stages (Fig. 4.3E), however SL is reduced ($p<0.05$) between pupal stage 3 and 5. Therefore, shaft filopodia morphogenesis is mainly caused by a reduction in the number of filopodia segments, but not by overall segment retraction. In contrast, the morphogenesis of tip filopodia is a combination of a reduction in segment number from pupal stage 3 to 4, and a collective retraction of filopodia at pupal stage 5, as tip filopodia SL is significantly reduced ($p<0.001$) from pupal stage 4 to 5 as compared to the stages 3 and 4 (Fig. 4.3E). The variation coefficient of SL shows that individual filopodia branch length is regulated in a narrow range compared to the number of branches and that regulation tightness does not change much during development (Fig. 4.3F). This is the case even for tip filopodia at pupal stage 5 when median segment length is significantly decreased. Longer segments have a clear

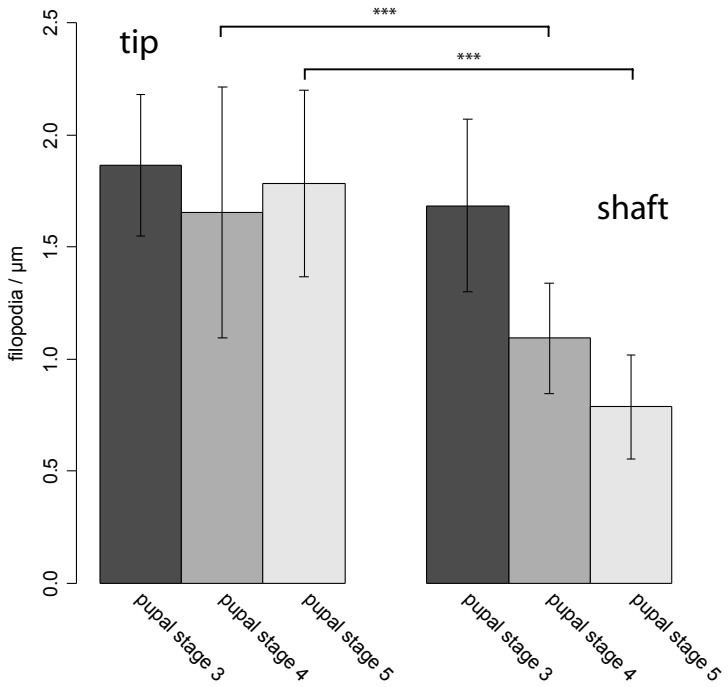

Figure 4.4: Filopodia frequency of occurrence along dendritic tip and shaft regions is regulated differentially during development. The mean density (filopodia / μm) is not changed during development at dendritic tip regions, however, is significantly down-regulated at dendritic shaft regions if compared to tip filopodia density. Error bar = standard deviation from mean; *** $p<0.001$.

tendency to be terminal segments of filopodia at tip as well as shaft filopodia areas (data not shown), however tip filopodia have a relative larger proportion of long segments than shaft filopodia. This is mirrored by the bigger VC of tip filopodia compared to shaft filopodia and might reflect a higher motility of tip filopodia.

4.4.7 Filopodia density is differentially regulated at dendritic tip and shaft areas during development

As filopodia vanish during the transition from pupal stage 5 to 6 with only few remedies, one should assume a reduction in SL during pupal stage 5 at any place, reflecting the retraction of filopodia segments. However, only dendritic tip filopodia show a significant reduction in SL from pupal stage 4 to 5. One possible explanation is that shaft filopodia are thinned out in such a smooth transition that the retraction of a subset of filopodia does not dominate the statistic evaluation of SL. Accordingly we evaluated the developmental regulation of filopodia density (number of filopodia / μm) along dendritic shaft and tip areas from pupal stage 3 to 5 (Fig. 4.4). Filopodia density at dendritic tips stays the same during filopodia dependent dendritic growth. Filopodia density at dendritic shafts, however, in fact decreases significantly ($p<0.001$) during development, already starting at pupal stage 4.

4.4.8 Analysis of synaptotagmin distribution along filopodia

It has been suggested that filopodia may play a critical role in synaptogenesis (Fiala et al., 1998; Yuste and Bonhoeffer, 2004). In the case of zebrafish tectal neurons they mediate synaptotrophic growth at dendritic tips (Niell et al., 2004) and synaptically induced local calcium signals have recently been shown to play a role in controlling filopodia growth in rat hippocampal neurons, proposing synaptic activity to be one regulation factor for filopodia density and morphogenesis (Lohmann et al., 2005). Different time courses of synaptogenesis at dendritic tip and shaft regions therefore might be one factor influencing filopodia density also in insects. However, in pyramidal neurons shaft and tip filopodia shape are regulated differentially by neuronal activity (Portera-Cailliau et al., 2003). Taken together, the functions of filopodia for synaptogenesis remain unclear. In particular, different mechanisms of synaptogenesis at different types and locations of filopodia within one dendritic tree have not been considered up to date, although different types of filopodia are found in pyramidal cells (Portera-Cailliau et al., 2003) and insect motorneurons (this study). Some filopodia bear synaptic contacts, as it has been demonstrated before by electron microscopy rat hippocampal neurons (Fiala et al., 1998). Are filopodia sites of synaptic contacts and are there rules for synapse distribution along filopodia at different stages of filopodia morphogenesis during postembryonic dendrite development? We tackle this question by mass-labeling presynaptic terminals with immuno-cytochemistry against synaptotagmin-like proteins and relate the distribution of putative presynaptic sites to the geometry of reconstructed filopodia. This is possible because dendritic trees of insect motorneurons, like MN5, are solely postsynaptic. Furthermore, electron microscopy has shown that in neuropil regions of the insect CNS the distribution of synapsin I-protein or synaptotagmin-protein spots, as visible on the light microscopy level, is correlated with clustered synaptic vesicles at synaptic sites (Watson and Schurmann, 2002). Therefore, the distribution of anti-synaptotagmin immunolabel along the dendritic surface is a good measure to identify loci likely to be presynaptic contact sites to the dendrite. For quantification at light microscopic resolution, we deploy newly developed methods for precise 3-dimensional reconstruction and co-localization analysis (Evers et al., 2005; Schmitt et al., 2004) of high resolution confocal image data (voxel size 120 $\times$ 120 $\times$ 300 nm). The methods are explained in detail elsewhere (Evers et al., 2005), but for clarity the general working scheme is briefly outlined in Fig. 4.5. Double labels of the motorneuron MN5 and synaptotagmin-antibody staining are acquired as confocal image stacks. Fig. 4.5*A1* shows a projection view of a dendritic segment with filopodia. This is reconstructed semi-automatically, yielding a tubular generalization of the projection

pattern, i.e. precise measures of midline run and radius (*A2*). Starting from the tubular reconstruction, a triangulated surface representation is calculated to best fit into the original staining distribution (Fig. 4.5*A3*), fully exploiting optical resolution and therefore surpasses previously available methods in accuracy (Evers et al., 2005). Fig. 4.5*B1* shows this surface reconstruction embedded into the 2^{nd} channel synaptotagmin-label, visualized as volume rendering. As superjacent image information above the reconstruction cannot be discriminated from synaptotagmin-staining in close surface vicinity, the volume rendering of synaptotagmin-label is restricted to 1μm distance to the reconstructed surface (Fig. 4.5*B2*). For quantification, the synaptotagmin staining density within 300 nm (i.e. summed staining intensity of voxels within 300 nm divided by the number of voxels) is calculated at every element of the triangulated surface reconstruction (a triangle) and depicted false-color coded in Fig. 4.5*B3*, with warmer colors representing higher synaptotagmin staining intensities. Although optical resolution of confocal light microscopy is not sufficient to fully prove synaptic connections by distance criteria between reconstructed neuronal surface and synaptotagmin-like immunoreactive profiles, clearly, high staining intensities of synaptotagmin-like proteins in direct vicinity (300nm) of purely postsynaptic dendritic surfaces stand for high synaptic contact probabilities. In contrast, zero staining excludes the presence of chemical presynaptic specialization (Evers et al., 2005). Accordingly previous work has demonstrated a strong correlation between putative input synapses into the dendritic tree of MN5 detected by this approach and electrophysiologically recorded synaptic inputs (Duch and Mentel, 2004). Therefore, we take the distribution of synaptotagmin staining density as a measure for synaptic contact probability along reconstructed dendritic surfaces. A similar approach has just been followed successfully (Lohmann et al., 2005), although only qualitatively at much lower optical resolution and smaller sample size.

To compare multiple reconstructions of filopodia from multiple animals, synaptotagmin staining density is scaled to values from 0 through 1, at which 0 is the smallest occurring value within the analyzed sub-volume around reconstructed tip/shaft areas, and 1 is biggest. This method is applied on the same reconstructions which are used to determine the metrics of filopodia morphogenesis. To illustrate the outcome exemplarily, the tubular reconstructions shown in Fig. 4.2 are used as initialization, and the resulting surface reconstruction are depicted in Fig. 4.5*C* to *G* (scale bar is 10 μm) false color-coded. Red indicates highest and blue lowest synaptotagmin staining intensities. Areas with high synaptotagmin density (warm colors) are indicated by arrows at dendritic segments and by arrowheads at filopodia. Some patches with high synaptotagmin density might be obscured by superjacent structures.

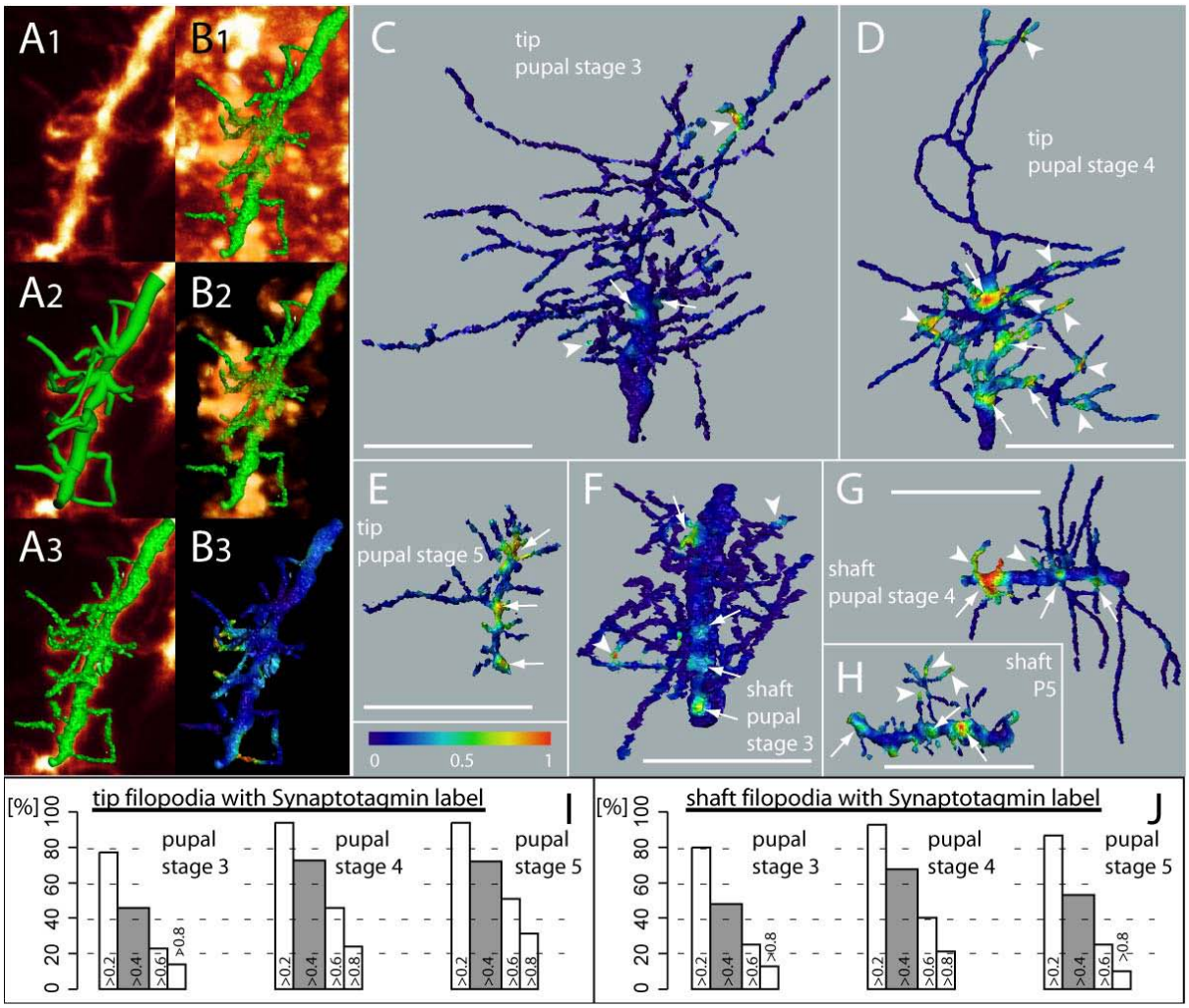

Figure 4.5: Analysis of synaptotagmin immuno-labeled profiles along filopodia by 3-dimensional reconstructions. Continued on next page.

At the beginning of dendritic growth at pupal stage 3, both tip (Fig. 4.5C) as well as shaft (Fig. 4.5F) filopodia have only little synaptotagmin staining in direct vicinity to their surface. One day later in development, at pupal stage 4, the amount of surface area touching putative presynaptic sites increases at tip (Fig. 4.5D) as well as shaft (Fig. 4.5G) filopodia. At pupal stage 5, synaptotagmin seems to be pronouncedly concentrated at tip dendrite segments (Fig. 4.5E), whereas the rare long shaft filopodia reach out to distant synaptotagmin positive volumes (Fig. 4.5H). Generally, only a subset of filopodia touches volumes with synaptotagmin staining, but the amount of filopodia contacting putative presynaptic partners increases with ongoing dendritic growth. This is quantified in Fig. 4.5I and J for dendritic tip and dendritic shaft filopodia respectively, plotting the percentage of filopodia touching Synaptotagmin-positive profiles. Because user defined threshold levels are error sensitive, the analysis was conducted using 4 different relative synapto-

Figure 4.5: continued

A Steps to generate precise surface reconstruction. Starting from confocal images (*A1*, projection view), a semi-automatic reconstruction method generates exact midline and diameter definitions (*A2*, tubular reconstructions) from dendrites and filopodia. As neuronal surface is not entirely round, a triangulated surface reconstruction is algorithmically determined to suite minor irregularities of neuronal surface. *B* Evaluation of synaptotagmin distribution. 2^{nd} channel image data of immuno-cytochemically labelled synaptotagmin is depicted as volume rendering in *B1*, embedding the precise surface reconstruction of *A3*. To examine the spatial correlation between neuronal surface and protein label, image information more distant than 1 μm is excised (*B2*). For quantification, staining density around all individual surface elements (triangles) is calculated within 300 nm and depicted false color-coded (blue= minimum (zero), red= maximum (100%) staining) in *B3*. Calculating the synaptotagmin distribution for all evaluated filopodia in Fig. 4.3, the result is exemplarily shown in *C*-*H* for the tubular reconstructions depicted in Fig. 4.2 *C*, *F* Pupal stage 3 synaptotagmin distribution at dendritic tip (*C*) and shaft (*E*). Only few surface patches with high synaptotagmin density are distributed along filopodia (arrow heads) and close to the dendrite (arrows) *D*, *G* Pupal stage 4 synaptotagmin distribution at dendritic tip (*D*) and shaft (*G*). synaptotagmin staining increased compared to pupal stage 3, and is pronouncedly concentrated close to the dendrite (arrows). At the dendritic tip (*D*) filopodia however seem to contact more distant synaptotagmin labels (arrow heads). *E*, *H* Pupal stage 5 synaptotagmin distribution at dendritic tip (*E*) and shaft (*H*). At tip filopodia synaptotagmin patches concentrate close to the dendrite (arrows, *E*). At pupal stage 5 shaft regions, synaptotagmin is accumulated close to the dendrite (*H*, arrows), but long-reaching shaft filopodia touch synaptotagmin-dense volumes (*H*, arrow heads). The percentage of filopodia touching synaptotagmin rich volumes is quantified in *I* for tip and in *J* for shaft regions, including all reconstructions used to determine filopodia metrics. To avoid error-prone single threshold definition, multiple relative thresholds are used (0.2; 0.4; 0.6; 0.8), however 0.4 (grey) includes synaptotagmin labels which just can be assessed by visual inspection. At tip regions (*I*), the percentage of filopodia touching synaptotagmin-rich volumes is continuously increased during development. At shaft regions (*J*), the peak percentage of filopodia touching synaptotagmin-rich volumes is already reached at pupal stage 4, and again decreases until pupal stage 5. Scale bars= 10 μm.

tagmin density levels (0.2; 0.4; 0.6; 0.8) as thresholds. The density level of 0.4, however, mirrors the lowest threshold level including structures which are clearly assessed as labeled structures if judged visually (grey bars, Fig. 4.5*I,J*). With ongoing development, the percentage of filopodia at dendritic tips touching synaptotagmin-positive volumes increases from pupal stage 3 to pupal stage 5. At shaft filopodia, however the highest percentage of filopodia, touching synaptotagmin-positive volumes is already reached in pupal stage 4. In the transition to the subsequent pupal stage 5, the percentage of shaft filopodia touching synaptotagmin-positive volumes yet decreases. This opposes the developmen-

tal process at tip filopodia, although the data are gathered within the same individual animals from the identical neurons. The observed developmental trends are similar at all four threshold levels, demonstrating that the described phenomena are not artifacts due to the selection of a specific threshold. The fact that synapse density is gradually increased at tip filopodia between pupal stage 3 and 5, but in contrast decreases at shaft filopodia from pupal stage 4 to 5 demonstrates that changes in synaptic density are not simply an artificial reflection of developmental changes in neuropil density.

4.4.9 Synaptotagmin staining density along filopodia decreases with midline distance from dendrite

We have shown a developmental change of the relative amount of filopodia touching synaptotagmin patches, and that this change follows different rules at dendritic tip and shaft areas. However, as filopodia are transient structures and are shortened during development (see above), presynaptic specializations touching filopodia must be transferred somehow to the dendrite in order to give them sustained function. This might happen by 3 possible mechanisms: (i) directed axonal growth towards the dendrite, (ii) replacement of filopodia carrying synapses by growing postsynaptic dendrites, or (iii) filopodia could be transformed into postsynaptic specialization, i.e. spines (Yuste and Bonhoeffer, 2004; Ziv and Smith, 1996). We are left with the first two options, because the MN5 does not posses spines. At dendritic tips, segments are added to the neuronal tree, principally enabling synaptotrophic growth of the postsynaptic dendrite. Dendritic shafts, however only grow little in diameter, requiring the translocation of presynaptic sites on filopodia towards the dendrite to sustain synaptic function.

To analyze the localization of synaptotagmin staining along the longitudinal projection axis of filopodia, and to average over a high number of filopodia at three subsequent developmental different stages, the distribution of relative staining density within 300 nm of the reconstructed surface along single filopodia is analyzed and related to its distance to the foot of the filopodium, measured along its curvilinear midline (midline distance). These density values are plotted as a function of midline distance in Fig. 4.6 as scatter plot. To allow the comparison of abstract data visualization in the scatter plot and its source, the synaptotagmin density map on surface reconstructions, the surface triangles of the reconstructions depicted in Fig. 4.5 are colored black in the respective plots of tip and shaft filopodia at different developmental ages in Fig. 4.6. Dendritic tip filopodia at pupal stage 3 extend into the surrounding neuropil, as if they were sampling for putative synaptic partners. Along this projection axis, a decrease of maximum relative

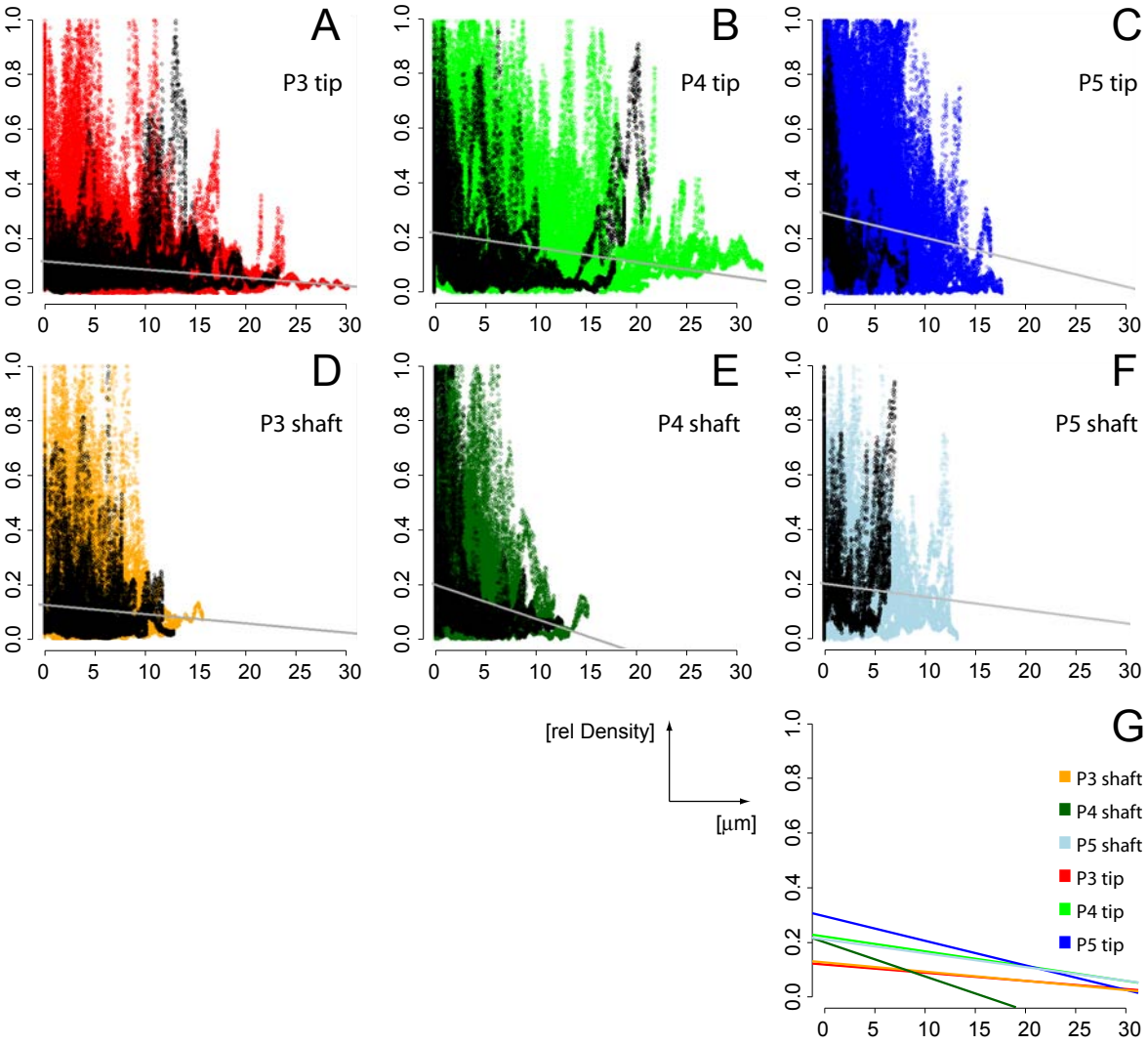

Figure 4.6: Synaptotagmin profiles accumulate at dendrites during development, however stronger at dendritic shaft than at tip regions. Continued on next page.

synaptotagmin staining density can be observed with increasing distance to the basis of the filopodium (Fig. 4.6*A*). This is true also for tip filopodia at pupal stage 4 with shorter MPL and TPL, however showing an overall increase of staining density at all distances (Fig. 4.6*B*). At pupal stage 5 dendritic tips with retracting filopodia and short MPL, maximal staining densities are found pronouncedly enriched at short distances from dendrites, however furthermost reaching filopodia still have lowest synaptotagmin staining density at their endings (Fig. 4.6*C*). This demonstrates that during dendritic growth and filopodia shortening, putative synaptic contacts become more and more translocated along filopodia towards dendrites. The situation found at dendritic shaft filopodia qualitatively resembles that at tip filopodia. The synaptotagmin staining density decreases

Figure 4.6: continued

This is shown quantitatively in *A*-*C* for tip filopodia, and in *D*-*F* for shaft filopodia. Synaptotagmin density (y-axis; summed intensity/volume) of every element of a triangulated surface reconstruction (a triangle) within 300 μm distance is plotted over its distance to the dendrite along the corresponding filopodia's curvilinear midline. Black data points originate from the respective reconstruction depicted in Fig. 4.5, allowing comparison between 3-dimensional structure and abstract data evaluation. Common to all developmental stages and locations within the dendritic tree is a decreasing synaptotagmin density along filopodia towards their distal endings. However, to compare the magnitude of these trends between developmental stages and locations respectively, linear regressions are fitted into the distribution (*A*-*F*, grey lines) and plotted combined in *G*. At pupal stage 3, tip (*A*) and shaft (*D*) filopodia start with the same average decrease of synaptotagmin density over distance. One day later in development (pupal stage 4), average synaptotagmin density decrease along filopodia becomes stronger at dendritic tip (*B*) and shaft (*E*) regions, yet more pronounced along shaft filopodia. This demonstrates a developmental accumulation of synaptotagmin close to the dendrite. At pupal stage 5, however the trend diverges. At dendritic tips (*C*), synaptotagmin accumulation close to the dendrite further increases. At shaft filopodia (*F*), however the decrease of synaptotagmin density along filopodia becomes less, suggesting synapse elimination to take place close to dendritic shafts from pupal stage 4 to 5.

with distance from the dendrite at pupal stage 3 (Fig. 4.6*D*), 4 (*E*) and 5 (*F*), however this translocation is accompanied by a smaller change of MPL and TPL as compared to tip filopodia.

Independent of the developmental stage or localization within the neuronal tree, a general feature of synaptotagmin staining density distribution is observed. At furthermost reaching filopodia endings, staining density is low. At intermediate distances filopodia show a gradually increasing span of relative synaptotagmin staining densities, and locations close to the origin of a filopodia show the highest staining densities.

4.4.10 Developmental translocation of synaptotagmin staining density along dendritic shaft and tip filopodia differs

To quantitatively compare synaptotagmin staining density decrease along filopodia between developmental stages of shaft and tip filopodia, linear regressions are fitted into the datasets (Fig. 4.6 *A* to *F*, summary in Fig. 4.6*G*). The y-axis intersection mirrors the amount of synaptotagmin staining; the slope however is giving the average degree of synaptotagmin density decrease along filopodia midline. Starting with newly born filopodia in P3 at dendritic tip (*dark red*) and shaft (*orange*) areas, y-axis intersection and slope are equal. This indicates that both types of "naïve" filopodia are confronted

with the same situation of immature neuropil. Looking one day later in development, at pupal stage 4 during ongoing synaptogenesis, the amount of filopodia touching synaptotagmin volumes increases equally at both, tip and shaft filopodia (compare Fig. 4.5*I,J*). The y-axis intersection increases similar at tip (*light green*) as well as shaft (*dark green*) filopodia, too. However the downward slope of synaptotagmin density distribution at shaft filopodia is noticeably steeper than at tip filopodia. Although y-axis intersection of tip filopodia further increases until pupal stage 5 (dark blue), the downward slope at this stage stays less than that of pupal stage 4 shaft filopodia. In contrast, the lower percentage of filopodia touching synaptotagmin volumes at shaft areas at pupal stage 5 (light blue) is accompanied by a decrease of downward slope, indicating synapse elimination close to the dendrite.

4.5 Discussion

This study investigates the role of filopodia in postembryonic remodelling of dendritic architecture in the intact central nervous system of insects during early metamorphosis. It shows that filopodia are densely distributed over the growing dendritic arbor during the outgrowth of the major central dendrites; however, at the same time during ongoing dendritic growth, filopodia undergo a morphogenic reduction in length and branching complexity. Two functional different types of filopodia exist, as presynaptic profiles translocate differentially towards the dendrite at different location within the dendritic tree: steering dendritic growth (dendritic tip filopodia) and directing axonal growth towards the dendrite (dendritic shaft filopodia).

4.5.1 Filopodia at dendritic tip and shaft regions have a different morphology

Deploying precise 3-dimensional reconstruction techniques of neuronal branching structure (Evers et al., 2005; Schmitt et al., 2004), we have shown four lines of morphological evidence for the existence of at least two distinct types of filopodia during early postembryonic dendritic morphogenesis, namely dendritic tip and shaft filopodia: (i) shaft filopodia are significantly shorter and less branched than tip filopodia, (ii) the density of shaft filopodia undergoes developmental down-regulation, whereas tip filopodia density stays constant, (iii) tip filopodia collapse during pupal stage 5, as indicated by a reduction in segment length, but shaft filopodia do not, and (iv) filopodia shape varies in a relative broader range at tip areas than at shaft filopodia, suggesting a tighter regulation at shaft

areas.

4.5.2 Filopodia morphogenesis

A recent study is in agreement with our results. It describes filopodia morphogenesis in mouse visual cortex slice preparation during early embryonic development by two photon live imaging (Portera-Cailliau et al., 2003), demonstrating a developmental shortening of filopodia and change of filopodia density in pyramidal neurons. We find a developmental decrease of filopodia length, and developmental reduction in filopodia branching complexity during postembryonic remodelling of denritic architecture (Fig. 4.2 and 4.3). In contrast to the findings in mouse visual cortex, we do not find a change in density of dendritic tip filopodia, but we show that the density of shaft filopodia is developmentally down-regulated during metamorphosis of *Manduca sexta* (Fig. 4.4).
In *Manduca sexta*, at pupal stage 3 filopodia emerge from the dendrite in parallel with a rising phase of the second peak of systemic ecdysteroid (Bollenbacher et al., 1981), and 20-Hydroxy-Ecdyson is shown to promote filopodia length and branching complexity in growth cones of *Manduca sexta* motorneuons *in vitro* (Matheson and Levine, 1999). Another factor inducing a stretch out of filopodia in invertebrates is nitric oxide (Bicker, 2005). However, regulation factors inducing a shortening of filopodia are not known in insects. There is evidence for a regulation of filopodia length and motility by presynaptic contact (Konur and Yuste, 2004) and synaptically induced activity (Lohmann et al., 2005; Portera-Cailliau et al., 2003) in vertebrates, however this could not yet be linked to the general level of synaptogenesis.

4.5.3 Synapses translocate along filopodia towards the dendrite during development

Is filopodia morphogenesis linked to synaptogenesis? We applied semi-automated 3-dimensional reconstruction techniques of neuronal surfaces and quantification of immuno-cytochemically stained proteins at full light microscopic resolution (Evers et al., 2005), and analyzed the distribution of immuno-cytochemically labeled synaptotagmin-like proteins along filopodia as a measure for presynaptic contact probability at large sample sizes (>1500 filopodia). We demonstrated a decrease of synaptotagmin staining intensity along filopodial projection axes at any stage or location within the Motorneuron 5 dendritic field as a general feature and showed a developmental increase of synaptotagmin accumulation along filopodia towards their proximal endings at the dendrite. However,

the degree and time course of synaptotagmin accumulation between dendritic tip and shaft filopodia differs. Dendritic tips grow into and occupy new neuropil regions from pupal stage 3 to 5, while synaptotagmin gradually accumulates along tip filopodia close to the dendrite. In contrast, dendritic shaft filopodia show a stronger accumulation of synaptotagmin staining during development compared to tip filopodia, however the peak of accumulation is already reached during pupal stage 4. At pupal stage 5, the degree of synaptotagmin accumulation at the proximal ending of shaft filopodia is again less than at pupal stage 4, suggesting synapse elimination to take place. In summary we have shown that filopodia. Morphogenesis goes along with the translocation of synaptotagmin profiles along filopodia towards dendrites.

How can such a translocation of synaptotagmin staining at dendrites occur? In case of dendritic tips, these actively grow into the maturating neuropil, probably extending towards presynaptic partners. Therefore endings of presynaptic axons would effectively be seen to be 'transferred' towards the postsynaptic dendrite, while the percentage of filopodia touching synaptotagmin-labeled volumes increases (Fig. 4.5*I*). At dendritic shaft regions however, the situation differs. Shaft dendrites could grow in diameter, which would shift filopodia along fixed axon terminals by a thickening of the dendrite. The growth in dendrite diameter however ranges only up to a few tens of microns, which is by far not enough to account for the observed relative translocation of synaptotagmin staining. An increase of synaptotagmin accumulation at shaft regions during dendrite outgrowth could also be induced by synaptotrophic steering of the dendritic tip, paving its way through the neuropil along synaptotagmin enriched volumes and therefore leaving dendritic shafts behind in synaptotagmin accumulations; however this would not explain that synaptotagmin accumulates stronger at dendritic shaft regions than at tips in pupal stage 4. Furthermore, the analyzed dendritic shaft regions are selected to be at least 10μm of unbranched dendritic segments (see above). Therefore, interstitial branching is not covered by our analysis and hence cannot account for the observed relative increase of synaptotagmin label at shaft regions. We end up with only two alternative possibilities at dendritic shafts: first, during reduction in filopodia density at shaft regions (Fig. 3.4), only those filopodia disappear, which are holding synaptic contacts at their distal endings, combined with a pruning of those not having synaptic contacts at all, which is needed to produce the demonstrated increase in the percentage of filopodia touching synaptotagmin-labeled volumes (Fig.4.5*J*). However it seems unlikely for a neuron to spend such energy expenditure forming numerous 5μm and longer filopodia reaching far out into the surrounding neuropil, anyway keeping only those filopodia with synapses close (<5μm) to the dendrite one day later in development. The second alternative is that

presynaptic axonal endings grow towards the postsynaptic dendrites, using the filopodia as guiding structures. This alternative seems to us the most plausible explanation for the demonstrated strong accumulation of synaptotagmin at dendritic shafts, in particular in the light of an increasingly dense packed neuropil when a converging presynaptic network must connect onto the Motorneuron 5 as its output neuron.
Because the degree of synaptotagmin accumulation close to the dendrite is less at dendritic tips than at shaft dendrites, this rules much for only one process to take place at dendritic tips, i.e. synaptotrophic growth of only the postsynaptic dendrite, rather than both, pre- and postsynaptic neuron, growing towards each other.

4.5.4 Different roles for different filopodia during dendritic development: steering of growth versus synaptogenesis

Local and transient increases of calcium concentration induced by synaptic activity is shown to stabilize filopodia projections or might even block new filopodia arising in close vicinity (Lohmann et al., 2005). On the other hand, different types of filopodia have been shown to react differently to synaptically induced activity (Portera-Cailliau et al., 2003). In the light of synaptic activity dependent filopodia regulation, filopodia morphogenesis and the developmental translocation of synaptotagmin profiles towards the dendrite can be combined into an appealing hypothesis: the advanced status of synaptogenesis at shaft filopodia compared to tip filopodia may control reduction in filopodia length, branching complexity and frequency of occurrence. Dendritic tip filopodia, however are faced with an earlier status of synaptogenesis, which would explain the lesser regulation of tip filopodia morphology, higher length and branching complexity and that tip filopodia density stays at a constant level during filopodia dependent dendritic growth. However, filopodia shortening during development is a general feature independent of their location within a dendritic tree, supposing also other factors which regulate filopodia morphogenesis.
A model for a dual function of dendritic filopodia has already been proposed in pyramidal neurons in mouse visual cortex for the steering of dendritic growth (tip filopodia) and synaptogenesis (shaft filopodia) (Portera-Cailliau et al., 2003). We propose an alike model for filopodia function during postembryonic dendritic growth in insects, however extend it by a localized relation to presynaptic axonal endings, which is summarized in Fig. 4.7. In the beginning of dendritic growth (pupal stage 3), dendritic filopodia reach out into the surrounding neuropil, making the first initial contacts to putative presynaptic partners at tip (Fig. 4.7*A*) as well as shaft (*D*) regions. On the next developmental step (pupal stage 4), dendritic tips grow into unoccupied neuropil regions, coarsely following filopodia

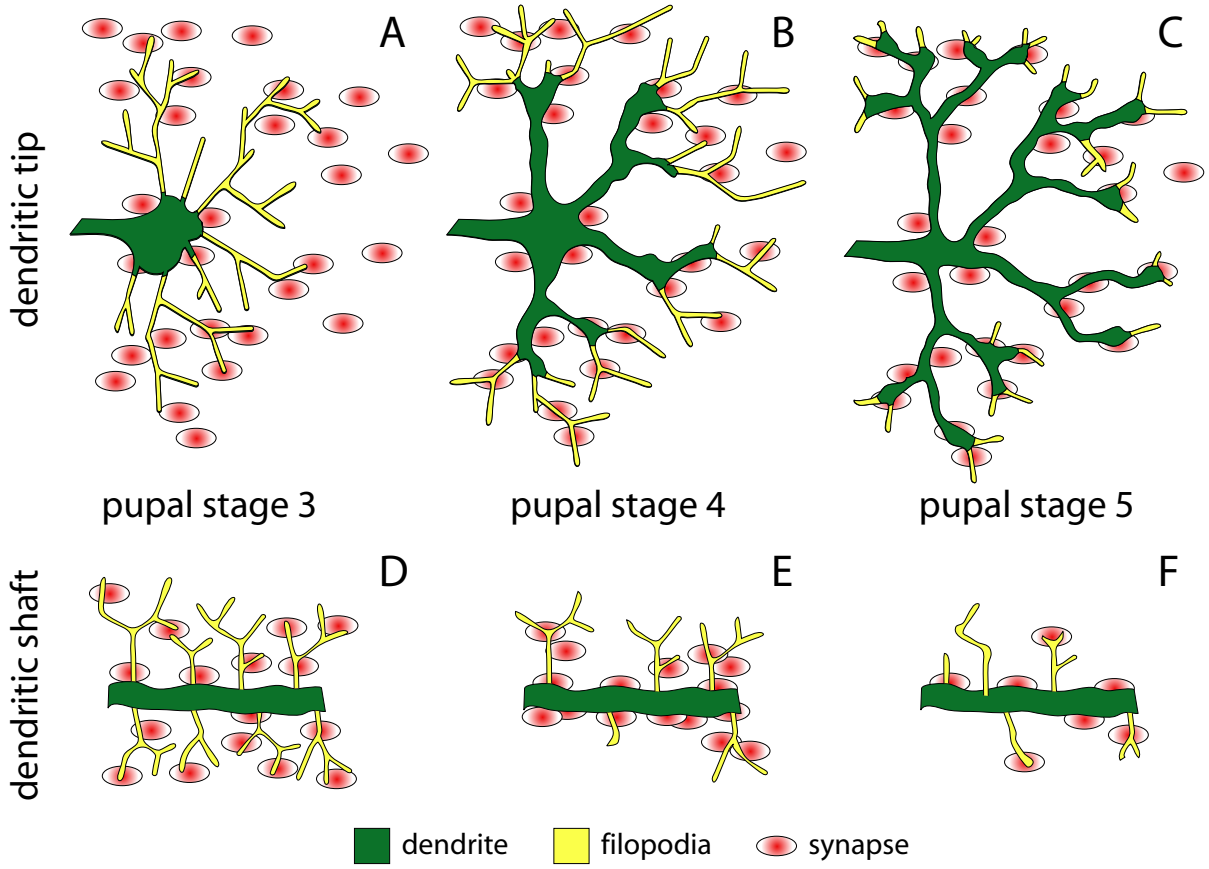

Figure 4.7: Model for dual filopodia function during dendritic growth. Green=dendrite; yellow=filopodia; red ellipse=synapse. For explanation, see discussion (4.5.4).

being stabilized by presynaptic contacts (synaptotrophic growth), while tip filopodia are shortened and their density is kept constant (B). These growing dendritic tips leave newly formed dendritic shaft regions behind, which are brought into reachable distance of the aimed presynaptic partners. Filopodia at shaft regions therefore take over the responsibility to guide the growth of presynaptic partner towards the dendrite, while filopodia density and length is reduced in parallel (E). First calcium transients induced at functional synapses might be one of the regulational factors inducing the reduction in filopodia branching complexity, length and density. At the time dendrites are reaching their maximal spatial extent during filopodia dependent synaptotrophic growth (pupal stage 5), dendritic tip filopodia collapse (C). At shaft regions, however, filopodia density has been further reduced in parallel with a reduction in synapse density, i.e. synapse elimination at the dendrite. However, some latecoming synaptic partners might still be contacted by filopodia, helping them to find the way towards the aimed postsynaptic dendrite (F). It seems plausible that synapse elimination by synaptic competition increases

the amount of mature synapses, therefore also might cause an increase of local calcium transients which further reduces filopodia density and length. Whether shaft filopodia are mediating a gliding in of presynaptic endings, or might pull them towards the dendritic segment (Fiala et al., 1998), cannot be decided upon our data.

4.5.5 Live imaging versus high resolution post-fixation confocal microscopy

Watching living tissue seems to be favorable for any type of biological investigation. Two-photon microscopy therefore appears to be the best solution to investigate neuronal growth, as it adds one decisive aspect: dynamics. Despite tremendous achievements made possible by two-photon imaging, there are also disadvantages. If the interaction between structural changes and proteins is of interest, the availability of fluorescently tagged proteins effectively restricts the scenario of practical use. Moreover, protein function could easily be disturbed if they are genetically tagged with fluorescent groups and culture condition might critically affect biological processes. In many cases, photo-toxicity paired with imaging speed and the amount of acquired image data restricts the observation of growth dynamics to small regions of individual cells. Also, optical resolution in z-dimension does not reach conventional confocal microscopy.
Analyzing fixed tissue by conventional confocal microscopy therefore still offers advantages over live imaging. Proteins can selectively be labeled by immuno-cytochemistry and imaging conditions can be optimized by specific tissue preparation without altering biological conditions. Moreover, high resolution confocal scans of whole neuronal ensembles are feasible. However, to deduce dynamic processes from static snapshot data generally needs a big sample size for statistic analysis. In this article, we have described the application of highly automated 3-dimensional image analysis, which significantly speeds up data evaluation, and therefore is one essential pre-requisite to answer this kind of questions in a reasonable time (Evers et al., 2005).

4.5.6 Methodological consideration

Synaptotagmins are an essential part of the calcium dependent vesicle release machinery at presynaptic sites; therefore immuno-cytochemical staining of synaptotagmin-like proteins serves a good measure of presynaptic localization. The meaning of varying staining intensities however is not clear. Whether synapse maturity is reflected in staining intensity or whether intense staining reflects a clustering of multiple presynaptic profiles can

only be speculated here. Certainly a synaptic contact cannot be confirmed without electron microscopy of the same region. However, places in neuropil with high synaptotagmin staining intensity in direct vicinity (300nm) to a purely postsynaptic dendritic surface (as is the case in insect motorneurons, (Watson and Schurmann, 2002)) still are indicating a high likelihood of presynaptic contact than at background staining intensity. Moreover, synaptic contacts on filopodia have been shown by electron microscopy (Fiala et al., 1998). Being aware of the problematic fact that we are dealing with synaptic probabilities rather than proven places of presynaptic contacts, we increased the sample size to over 200 single filopodia at any stage or location to have a statistical relevant set of data.

Grants

We gratefully acknowledge the support by the Deutsche Forschungsgemeinschaft to J. F. Evers and C. Duch (SFB 515, A7) and to D. Münch (GRK 120).

References

Bell, R. A. and Joachim, F. G. (1976). Techniques for rearing laboratory colonies of tobacco hornworms and pink bollworms lepidoptera-sphingidae- gelechiidae. *Ann. Entomol. Soc. Am.*, 69(2):365–373.

Bicker, G. (2005). Stop and go with no: Nitric oxide as a regulator of cell motility in simple brains. *Bioessays*, 27(5):495–505.

Bollenbacher, W. E., Smith, S. L., Goodman, W., and Gilbert, L. I. (1981). Ecdysteroid titer during larval-pupal-adult development of the tobacco hornworm, *Manduca sexta*. *Gen. Comp. Endocrin.*, 44(3):302–306.

Consoulas, C., Duch, C., Bayline, R. J., and Levine, R. B. (2000). Behavioral transformations during metamorphosis: remodeling of neural and motor systems. *Brain Res. Bull.*, 53(5):571–583.

Dubuque, S. H., Schachtner, J., Nighorn, A. J., Menon, K. P., Zinn, K., and Tolbert, L. P. (2001). Immunolocalization of synaptotagmin for the study of synapses in the developing antennal lobe of *Manduca sexta*. *J. Comp Neurol.*, 441(4):277–287.

Duch, C. and Levine, R. B. (2000). Remodeling of membrane properties and dendritic ar-

chitecture accompanies the postembryonic conversion of a slow into a fast motoneuron. *J. Neurosci.*, 20(18):6950–6961.

Duch, C. and Mentel, T. (2004). Activity affects dendritic shape and synapse elimination during steroid controlled dendritic retraction in *Manduca sexta*. *J. Neurosci.*, 24(44):9826–9837.

Evers, J. F., Schmitt, S., Sibila, M., and Duch, C. (2005). Progress in functional neuroanatomy: Precise automatic geometric reconstruction of neuronal morphology from confocal image stacks. *J. Neurophysiol.*, 93(4):2331–2342.

Fiala, J. C., Feinberg, M., Popov, V., and Harris, K. M. (1998). Synaptogenesis via dendritic filopodia in developing hippocampal area ca1. *J. Neurosci.*, 18(21):8900–8911.

Gomez, T. M., Dagan, D., and Spitzer, N. C. (1999). Regulation of growth cone cytoskeletal dynamics by calcium transients. *Mol. Biol. Cell*, 10:27A.

Gomez, T. M., Robles, E., Poo, M. M., and Spitzer, N. C. (2001). Filopodial calcium transients promote substrate- dependent growth cone turning. *Science*, 291(5510):1983–1987.

Gomez, T. M. and Spitzer, N. C. (2000). Regulation of growth cone behavior by calcium: new dynamics to earlier perspectives. *J. Neurobiol.*, 44(2):174–183.

Kater, S. B. and Shibata, A. (1994). The unique and shared properties of neuronal growth cones that enable navigation and specific pathfinding. *J. Physiol Paris*, 88(3):155–163.

Konur, S. and Yuste, R. (2004). Imaging the motility of dendritic protrusions and axon terminals: roles in axon sampling and synaptic competition. *Mol. Cell. Neurosci.*, 27(4):427–440.

Levine, R. B., Morton, D. B., and Restifo, L. L. (1995). Remodeling of the insect nervous system. *Curr. Opin. Neurobiol.*, 5(1):28–35.

Levine, R. B. and Weeks, J. C. (1996). Cell culture approaches to understanding the actions of steroid hormones on the insect nervous system. *Dev. Neurosci.*, 18(1-2):73–86.

Libersat, F. and Duch, C. (2002). Morphometric analysis of dendritic remodeling in an identified motoneuron during postembryonic development. *J. Comp Neurol.*, 450(2):153–166.

Lohmann, C., Finski, A., and Bonhoeffer, T. (2005). Local calcium transients regulate the spontaneous motility of dendritic filopodia. *Nat. Neurosci.*, 8(3):305–312.

Matheson, S. F. and Levine, R. B. (1999). Steroid hormone enhancement of neurite outgrowth in identified insect motor neurons involves specific effects on growth cone form and function. *J. Neurobiol.*, 38(1):27–45.

Niell, C. M., Meyer, M. P., and Smith, S. J. (2004). In vivo imaging of synapse formation on a growing dendritic arbor. *Nat. Neurosci.*, 7(3):254–260.

Portera-Cailliau, C., Pan, D. T., and Yuste, R. (2003). Activity-regulated dynamic behavior of early dendritic protrusions: evidence for different types of dendritic filopodia. *J. Neurosci.*, 23(18):7129–7142.

R Development Core Team (2004). *R: A language and environment for statistical computing*. R Foundation for Statistical Computing, Vienna, Austria. ISBN 3-900051-07-0.

Rehder, V. and Kater, S. B. (1992). Regulation of neuronal growth cone filopodia by intracellular calcium. *J. Neurosci.*, 12(8):3175–3186.

Rehder, V. and Kater, S. B. (1996). Filopodia on neuronal growth cones: Multi-functional structures with sensory and motor capabilities. *Seminars in the Neurosciences*, 8(2):81–88.

Reinecke, J. P., Buckner, J. S., and Grugel, S. R. (1980). Life-cycle of laboratory-reared tobacco hornworms, *Manduca sexta* - study of development and behavior, using time-lapse cinematography. *Biol. Bull.*, 158(1):129–140.

Robles, E., Gomez, T. M., and Spitzer, N. C. (1999). Global and local growth cone calcium transients promote axon turning at substrate borders in vitro. *Mol. Biol. Cell*, 10:451A.

Schmitt, S., Evers, J. F., Duch, C., Scholz, M., and Obermayer, K. (2004). New methods for the computer-assisted 3-d reconstruction of neurons from confocal image stacks. *Neuroimage.*, 23(4):1283–1298.

Tissot, M. and Stocker, R. F. (2000). Metamorphosis in drosophila and other insects: the fate of neurons throughout the stages. *Progress in Neurobiology*, 62(1):89–111.

Tolbert, L. P., Matsumoto, S. G., and Hildebrand, J. G. (1983). Development of synapses in the antennal lobes of the moth *Manduca sexta* during metamorphosis. *J. Neurosci.*, 3(6):1158–1175.

Truman, J. (1990). Metamorphosis of the insect nervous system. In Gilbert, L., Tata, J., and Atkinson, B., editors, *Metamorphosis: postembryonic reprogramming of gene expression in amphibian and insect cells*, pages 283–320. Academic, San Diego.

Vaughn, J. E. (1989). Fine-structure of synaptogenesis in the vertebrate central nervous-system. *Synapse*, 3(3):255–285.

Watson, A. H. and Schurmann, F. W. (2002). Synaptic structure, distribution, and circuitry in the central nervous system of the locust and related insects. *Microsc. Res. Tech.*, 56(3):210–226.

Weeks, J. C. and Truman, J. W. (1986). Hormonally mediated reprogramming of muscles and motoneurons during the larval pupal transformation of the tobacco hornworm, manduca-sexta. *J. Exp. Biol.*, 125:1–13.

Wouterlood, F. G., Van Denderen, J. C. M., Blijleven, N., Van Minnen, J., and Hartig, W. (1998). Two-laser dual-immunofluorescence confocal laser scanning microscopy using cy2- and cy5-conjugated secondary antibodies: unequivocal detection of co- localization of neuronal markers. *Brain Research Protocols*, 2(2):149–159.

Yuste, R. and Bonhoeffer, T. (2004). Genesis of dendritic spines: insights from ultrastructural and imaging studies. *Nat. Rev. Neurosci.*, 5(1):24–34.

Ziv, N. E. and Smith, S. J. (1996). Evidence for a role of dendritic filopodia in synaptogenesis and spine formation. *Neuron*, 17(1):91–102.